Size dependence of nanoparticle dissolution in a matrix: Gold in bismuth

P. Swaminathan, S. Sivaramakrishnan, J. S. Palmer, and J. H. Weaver
Department of Materials Science and Engineering, University of Illinois at Urbana-Champaign, Urbana, Illinois 61801, USA
(Received 24 December 2008; revised manuscript received 5 March 2009; published 17 April 2009)

We discuss the dissolution of Au nanoparticles in a Bi matrix. The particles were produced by vapor deposition at room temperature, and they burrowed to minimize their free energy. Using *in situ* transmission electron microscopy, we measured the rate of dissolution as a function of particle size and deduced the activation energy for this process. We also followed the structural changes in the system by high-resolution electron microscopy and nanobeam diffraction. This study develops an important understanding of the dependence of size on the stability and reactivity of nanoparticles.

DOI: 10.1103/PhysRevB.79.144113 PACS number(s): 64.70.Nd, 68.35.−p, 68.37.Og, 61.05.jm

The dissolution of an unstable second phase (precipitate) in a stable matrix dictated by bulk thermodynamics has been studied extensively.[1–3] As has been demonstrated, precipitate sizes, compositions, densities, and distributions affect the dissolution kinetics. Dissolution cannot be modeled simply as the antithesis of growth due to differences in time evolution of the solute concentration profile across the precipitate-matrix interface.[1]

Recent theoretical studies have shown deviations from the bulk phase behavior for small particles, and this affects precipitate formation and dissolution.[4,5] Size affects phase transformations by changing the solid solubility of components,[6,7] introducing metastable phases,[8] and/or lowering the transformation temperature.[9] Transformation kinetics are also enhanced due to modified diffusion channels.[10,11] Size enters through the decreased coordination of atoms at the curved interface which leads to an increased solute concentration given by the Gibbs-Thompson equation.[12] Size effects have been observed for supported nanoparticles, where depressions in melting and evaporation temperatures reflect increased vapor pressures around a curved surface.[13] The dependence of reactivity on size can be used to obtain their free energies,[14] and this has applications in variety of areas including catalysis.[15]

Recently, we showed that kinetic processes associated with growth and burrowing make it possible to assess the significance of the latter on the size distribution of Au particles formed during the deposition of Au on Bi.[16] During atom deposition at room temperature, Au clusters nucleate and grow but—because of energy considerations—they burrow into the film after reaching sizes at which concepts such as surface and interface energies become meaningful. Because this different pathway leads to metastable nanoparticles in a matrix, we are now able to follow the second step in the thermodynamic pathway, namely, the dissolution of these particles. In this paper, we examine the size and temperature dependencies of that dissolution using *in situ* transmission electron microscopy (TEM). From the rate of dissolution, we are able to deduce the energetics of this process. We also examined the phase transformations using nanobeam electron diffraction (NBED) and followed structural changes in individual particles using high-resolution TEM (HRTEM).

Sample preparation was performed in an ultrahigh vacuum chamber with a base pressure below 1×10^{-9} Torr. The substrates were amorphous carbon (*a*-C) TEM grids degassed at 200 °C for 5 min and then subsequently heated during the chamber bake. Bi films were grown at room temperature by vapor deposition at the rate of 1 nm/min. The films were polycrystalline with preferential (001) orientation and lateral grain sizes 3 to 4 times the film thickness, consistent with normal grain growth.[17] Au was vapor deposited onto the Bi at a rate of ~0.1 nm/min at room temperature.

Particle distributions were obtained using a 120 keV Philips CM 12 TEM. For *in situ* annealing studies, the sample was heated to the desired temperature and held for a short time (typically 10 min) to minimize thermal drift before recording images at that temperature. Annealing experiments were performed in the range 130–170 °C. Structural changes, in a randomly chosen area in the sample, were then imaged at regular intervals to determine the rates of change in particle radii. Measurements of the rates were carried out at low magnification so that the electron beam was defocused to spread over a large area and sample heating was less than 4 °C.[18] This is important because beam heating can cause melting and phase transformations.[19,20]

High-resolution imaging and NBED during annealing were obtained in a 200 keV JEOL 2010F scanning transmission electron microscope [(S)TEM] and a 200 keV JEOL 2010 LaB_6 TEM, respectively. The JEOL 2010 (S)TEM uses a field-emission gun to generate a large electron flux, which is essential for high-resolution imaging. NBED was chosen over conventional selected area diffraction because it can obtain structural information from nanometer-sized regions by using a special condenser lens that generates a nanometer-sized parallel electron beam.[21–23] This enables us to obtain a comparable signal from the Au nanoparticles and the underlying Bi film with sufficient beam intensity to gain information from the nanoparticles.

As discussed in Ref. 16, free-energy differences for Au and Bi indicate that it is favorable for Au particles to be buried in Bi rather than supported on the surface. This state is metastable below 116 °C and a two-phase system derived from Au_2Bi and Bi is stable above 116 °C.[24] By annealing the samples, we can accelerate the kinetics of dissolution so that real time measurements are possible. For example, Fig. 1 shows the dissolution of Au particles embedded in Bi during annealing at 160 °C. The particles were formed by depositing 1.5 nm Au on a 20-nm Bi film at room temperature. This gives particles with an average radius of

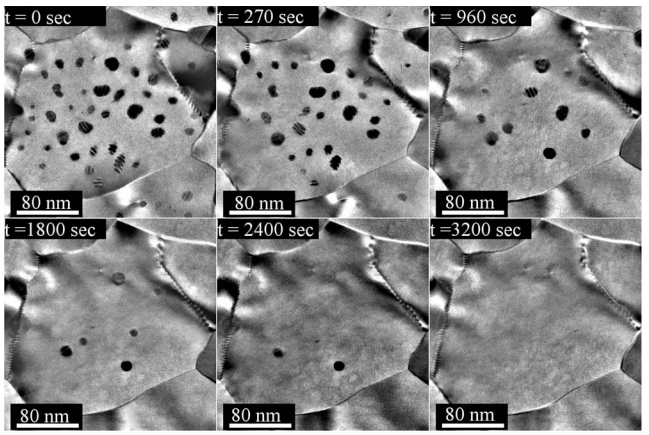

FIG. 1. TEM images of Au particles embedded in Bi at 160 °C showing that they dissolved and ultimately disappeared. The disappearance time was roughly proportional to the particle size. Changes to the Bi film were negligible.

5.14 ± 2.06 nm and density $\sim 10^{11}$ cm^{-2}, with a typical particle containing ~30 000 atoms. Analysis showed that the disappearance time was roughly related to the particle size. Similar results were obtained between 130 °C and 170 °C. The disappearance time decreased with increasing temperature for particles of a given size, indicating a thermally activated process. No Au precipitates appeared during cooling, indicating that the solid solubility of Au in Bi was not exceeded, and there were no changes in the Bi films. We also carried out annealing experiments in the growth chamber, prior to imaging, to confirm that dissolution occurred in the absence of the electron beam (annealed at 150 °C for 1 h).

The high-resolution TEM images of Fig. 2 show the structural changes of a Au particle at 130 °C over an interval of 25 min. The Bi lattice had a d spacing of 0.227 nm corresponding to (110) planes. The Au particle had an initial radius of 8 nm with d spacing of 0.236 nm corresponding to (111) planes. Thus, the Au-Bi lattice mismatch for this particle was 3.8% and the interface was incoherent. This difference in the in-plane d spacing led to the formation of moiré

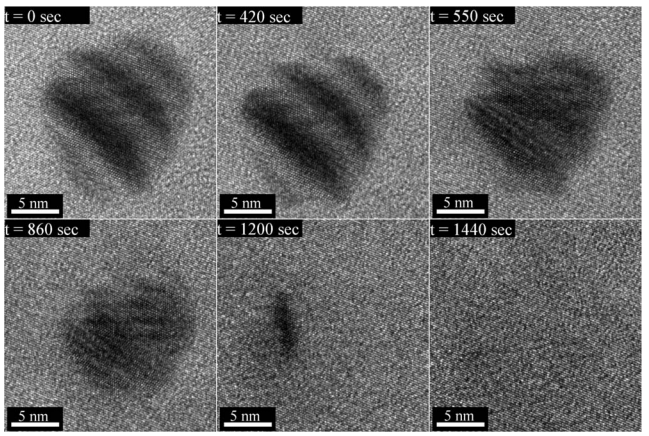

FIG. 2. HRTEM images of a Au particle at 130 °C collected over a 25 min period. The particle orientation, as measured by the spacing in the moiré pattern in the first two images, and the in-plane spacing do not change.

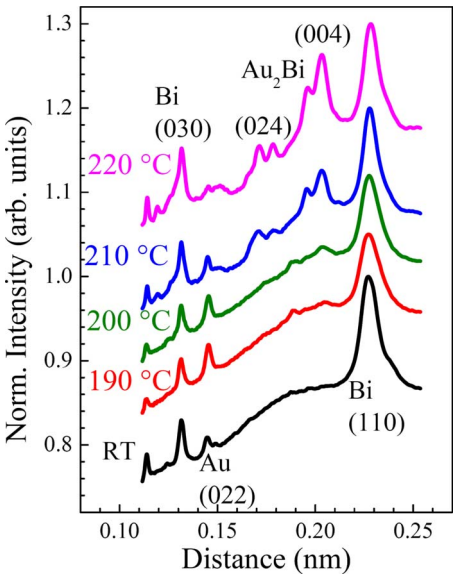

FIG. 3. (Color online) NBED data during a constant rate heating experiment. The data are plotted as normalized intensity vs distance, vertically displaced for clarity. The Au particles were formed by depositing 1 nm of the material on 20 nm Bi. The annealing rate was 3 °C/min. Initially, at room temperature, peaks corresponding to Bi and Au are visible. With an increase in temperature Au peaks go down in intensity and ultimately disappear, while new peaks corresponding to Au_2Bi are formed. No visible changes are observed in the Bi peaks.

patterns,[25] which are manifest as fringes in the particle with a center to center spacing of 5.5 nm. The lattice spacing did not change as the particle size decreased. Scanning across the interface also indicated that an abrupt transition from Au to Bi was maintained, i.e., there was no reorientation or shrinking of the spacing in the particle to match with the Bi lattice and the interface remained incoherent. In Fig. 2, the moiré patterns were visible in the first two images but became less clear as the particle dissolved.

The annealing experiments described above were carried out above the bulk equilibrium formation temperature of Au_2Bi (116 °C).[24] Hence, the disappearance of the Au particles should be related to the formation of Au_2Bi. To confirm this, we performed NBED experiments during heating at a constant rate of 3 °C/min. Figure 3 summarizes the NBED data as plots of normalized diffraction intensity vs distance [using the Bi (110) peak as reference]. The data were collected from a random area in the sample containing an ensemble of Au nanoparticles embedded in a Bi grain. The particles were formed by depositing 1 nm Au on 20 nm Bi. The peaks for Bi correspond to diffraction from (001) zone axis grains. With increased temperature, the Au peak decreased and ultimately disappeared as peaks corresponding to Au_2Bi appeared. No changes were evident in the Bi features, and none were expected below the melting point (270 °C). The sample was constantly monitored and corrected for thermal drift during this measurement.

The NBED and high-resolution TEM results indicate that the particles disappear due to the solubility of Au in Bi at elevated temperatures, with Au_2Bi formation occurring in a

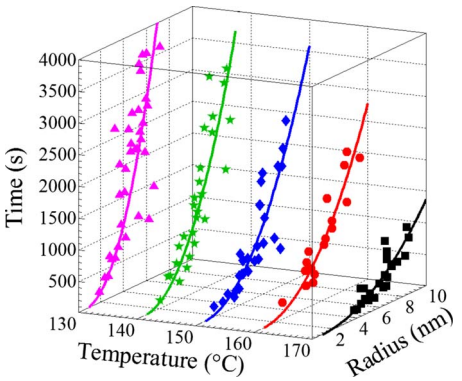

FIG. 4. (Color online) Plot of the disappearance time as a function of particle radius and temperature. The disappearance time defined as the first TEM image in which the particle is no longer visible is obtained from TEM images such as those of Fig. 1. The time increases nonlinearly with particle size but decreases with temperature for particles of a given size. The lines through the data points represent fits obtained using Eq. (4).

spatially separate region. In order to quantify the dissolution process, we determined the rate of change in particle size with temperature through TEM images in a fixed area in the sample. Figure 1 represents the results from one such measurement, and the data in Fig. 4 summarize the results for particles of different sizes. The disappearance time is defined as the time stamp of the first TEM image when the particle is not seen. This time increases nonlinearly with size and decreases with temperature for a given size, as expected for a thermally activated process.

To model the dissolution process, we used a modified form of a one-dimensional diffusion equation originally used by Aaron and Kotler[1] to study the dissolution of micron-sized precipitates in a matrix. A similar formalism was adopted by Morgenstern *et al.*[26] in their analysis of decay of bilayer Ag islands on Ag (111). Our system is three-dimensional spherical particles embedded in a matrix. The rate of decay of a particle is

$$\frac{dR}{dt} = -2\frac{C_I}{C_P}\left(\frac{D}{R}\right), \tag{1}$$

where C_I is the concentration of the solute at the interface between the solute and matrix and C_P is the concentration of the solute in the precipitate. D is the diffusivity of solute atoms in the matrix and R and t represent particle radius and time, respectively. The curvature of the particle leads to an increase in the solute concentration at the interface compared to a bulk phase $[C_I(\infty)]$. This increase is given by the Gibbs-Thompson equation[12]

$$C_I(R) = C_I(\infty)\exp\left(\frac{\gamma V_p}{k_B T R C_P}\right), \tag{2}$$

where γ is the particle interfacial energy, V_p is the molar volume of the precipitate, and k_B is the Boltzmann constant. From Eqs. (1) and (2)

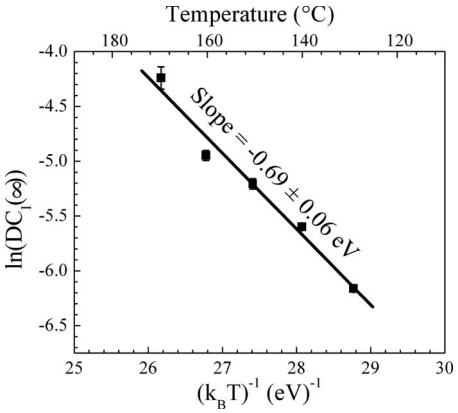

FIG. 5. The slope of $\ln[DC_I(\infty)]$ vs $(k_BT)^{-1}$ gives the activation energy of dissolution, where $DC_I(\infty)$ was obtained from the fits of the dissolution time to the particle radius at different temperatures, using Eq. (4). The energy of 0.69 eV represents the total energy for an Au atom to detach from the particle and diffuse into the matrix.

$$\frac{dR}{dt} = -2\frac{C_I(\infty)}{C_p}\frac{D}{R}\exp\left(\frac{\gamma V_p}{k_B T R C_p}\right). \tag{3}$$

Solving to get the total time required for a particle of initial size R_0 $(t=0)$ to dissolve completely $(R=0,\ t=t_f)$ gives

$$t_f = \frac{C_p}{4DC_I(\infty)}\left[\frac{\beta^2\gamma^2}{T^2}\Gamma\left(0, \frac{\beta\gamma}{R_0 T}\right) - R_0\left(\frac{\beta\gamma}{T} - R_0\right)\exp\left(-\frac{\beta\gamma}{R_0 T}\right)\right],$$

$$\beta = \frac{V_p}{k_B C_P}. \tag{4}$$

Here, Γ represents the gamma function and the other terms have the same meaning as given above. Equation (4) can be fitted to the experimental dissolution time. V_p is the molar volume of Au, 16.9×10^{-3} nm^3. C_p the solute concentration of the precipitate is 1 since the precipitate is pure Au. For the interfacial free energy of a Au particle in Bi γ, we used 0.46 J m^{-2}.[16] The fits in Fig. 4 can be used to obtain $DC_I(\infty)$. The bulk solubility and diffusivity of Au in Bi are not known and, hence, it is not possible to separate the two terms. However, each term can be written as the product of a pre-exponential part and an activation energy. Accordingly, a plot of $\ln[DC_I(\infty)]$ vs $(k_BT)^{-1}$ should be linear with a slope of $-E_a$, which represents the total activation energy for dissolution. From Fig. 5, we conclude that this value is 0.69 ± 0.06 eV.

This activation energy is the sum of the dissolution [represented by $C_I(\infty)$] and the diffusion barrier (represented by D). For coherently formed precipitates, the decay occurs by the formation and movement of ledges.[2] A similar decay mechanism was observed for homoepitaxial two-dimensional (2D) Ag islands[27] with an activation energy of 0.71 eV for an atom to detach from a single height step. For Au-Bi, with an incoherent interface, the ledge mechanism can be ruled out. However, vacancies are formed during the burrowing of the

Au particle due to the disordered motion of atoms at the interface.[28] Hence, the dissolution likely occurs by atoms moving from the particles into vacancy sites and then diffusion into the matrix. The dissolution energy can be estimated by multiplying the interfacial energy of the particle in the matrix 0.46 J m^{-2}, by the area per atom ~0.07 nm^2, giving a value of ~0.20 eV (entropy effects in the particle are minimal, since we are much lower than the melting point of Au). Since the total activation energy is 0.69 eV, the difference 0.49 eV is the energy required for an Au atom to diffuse from the interface. An estimate of the activation energy for the bulk diffusion of Au in Bi obtained from melting point correlations gives ~1.5 eV.[29] This is much higher than the activation energy obtained from our dissolution experiments. Special diffusion channels have been observed in thin films, e.g., Ostwald ripening of Si nanoparticles in Al proceeds by diffusion along dislocation cores, lowering the activation energy compared to the bulk diffusion.[10] It is possible that similar mechanisms are active here; the higher vacancy concentration at the Au-Bi interface could be responsible for the lowering of the activation energy for diffusion.

In the above, we were able to follow the dissolution of Au particles embedded in a Bi matrix. We calculated the activation energies for this process by using a one-dimensional diffusion equation to fit the rates as a function of particle size and temperature. The formation of a solid solution of Au in Bi acts as a precursor for the formation of the Au_2Bi. Studies of nanoparticle dissolution in systems, where the bulk solubility is known, can be used to obtain the size-dependent free energy of nanoparticles.

TEM measurements were carried out in the Frederick Seitz Materials Research Laboratory Central Facilities, University of Illinois, which are partially supported by the U.S. Department of Energy under Grants No. DE-FG02-07ER46453 and No. DE-FG02-07ER46471.

[1] H. B. Aaron and G. R. Kotler, Metall. Trans. **2**, 393 (1971).
[2] W. E. Benson and J. M. Howe, Philos. Mag. A **75**, 1641 (1997).
[3] L. M. Cheng, E. B. Hawbolt, and T. R. Meadowcroft, Metall. Mater. Trans. A **31**, 1907 (2000).
[4] M. Wautelet, J. P. Dauchot, and M. Hecq, Nanotechnology **11**, 6 (2000).
[5] J. Park and J. Lee, CALPHAD: Comput. Coupling Phase Diagrams Thermochem. **32**, 135 (2008).
[6] A. S. Shirinyan, A. M. Gusak, and M. Wautelet, Acta Mater. **53**, 5025 (2005).
[7] C. T. Schamp and W. A. Jesser, Metall. Mater. Trans. A **37**, 1825 (2006).
[8] C. W. Hills, N. H. Mack, and R. G. Nuzzo, J. Phys. Chem. B **107**, 2626 (2003).
[9] G. Ouyang, X. Tan, C. X. Wang, and G. W. Yang, Chem. Phys. Lett. **420**, 65 (2006).
[10] M. Legros, G. Dehm, E. Arzt, and T. J. Balk, Science **319**, 1646 (2008).
[11] H. Yasuda and H. Mori, Phys. Rev. Lett. **69**, 3747 (1992).
[12] M. Perez, Scr. Mater. **52**, 709 (2005).
[13] K. K. Nanda, F. E. Kruis, and H. Fissan, Phys. Rev. Lett. **89**, 256103 (2002).
[14] Q. Jiang and H. M. Lu, Surf. Sci. Rep. **63**, 427 (2008).
[15] C. T. Campbell, S. C. Parker, and D. E. Starr, Science **298**, 811 (2002).
[16] P. Swaminathan, J. S. Palmer, and J. H. Weaver, Phys. Rev. B **78**, 115416 (2008).
[17] C. V. Thompson, Annu. Rev. Mater. Sci. **20**, 245 (1990).
[18] D. D. Thornburg and C. M. Wayman, Phys. Status Solidi A **15**, 449 (1973).
[19] T. Yokota, M. Murayama, and J. M. Howe, Phys. Rev. Lett. **91**, 265504 (2003).
[20] D. Ugarte, Nature (London) **359**, 707 (1992).
[21] J. M. Zuo, M. Gao, J. Tao, B. Q. Li, R. Twesten, and I. Petrov, Microsc. Res. Tech. **64**, 347 (2004).
[22] J. M. Zuo and B. Q. Li, Phys. Rev. Lett. **88**, 255502 (2002).
[23] W. J. Huang, R. Sun, J. Tao, L. D. Menard, R. G. Nuzzo, and J. M. Zuo, Nature Mater. **7**, 308 (2008).
[24] C. Servant, E. Zoro, and B. Legendre, CALPHAD: Comput. Coupling Phase Diagrams Thermochem. **30**, 443 (2006).
[25] M. De Graef, *Introduction to Conventional Transmission Electron Microscopy* (Cambridge University Press, Cambridge, 2003).
[26] K. Morgenstern, G. Rosenfeld, and G. Comsa, Phys. Rev. Lett. **76**, 2113 (1996).
[27] K. Morgenstern, G. Rosenfeld, E. Laegsgaard, F. Besenbacher, and G. Comsa, Phys. Rev. Lett. **80**, 556 (1998).
[28] J. Frantz and K. Nordlund, Phys. Rev. B **67**, 075415 (2003).
[29] A. M. Brown and M. F. Ashby, Acta Metall. **28**, 1085 (1980).